

Tight-binding piezoelectric theory and electromechanical coupling correlations for transition metal dichalcogenide monolayers

Yunhua Wang,^{1,2,*} Zongtan Wang,³ Jie Li,³ Jie Tan,¹ Biao Wang,^{1,2,†} and Yulan Liu^{3,‡}

¹Sino-French Institute of Nuclear Engineering and Technology, Sun Yat-sen University, Zhuhai 519082, China

²State Key Laboratory of Optoelectronic Materials and Technologies, School of Physics, Sun Yat-sen University, Guangzhou 510275, China

³School of Engineering, Sun Yat-sen University, Guangzhou 510006, China



(Received 3 January 2018; revised manuscript received 9 April 2018; published 4 September 2018)

The lack of inversion symmetry in semiconducting transition metal dichalcogenide monolayers (TMDMs) enables a considerable intrinsic piezoelectricity, which opens prospects for atomically thin piezotronics and optoelectronics. Here, based on the tight-binding (TB) approach and Berry phase expression for electronic polarization difference, we establish an atomic-scale TB theory for demonstrating piezoelectric physics in TMDMs. Using the TB piezoelectric theory, we predict the electronic Grüneisen parameter (EGP), which measures the electron-phonon couplings for TMDMs. By virtue of the constructed analytical piezoelectric model, we further reveal the correlation between the electronic contribution to piezoelectric coefficients and strain-induced pseudomagnetic gauge field (PMF). These predicted EGP and PMF for TMDMs are experimentally testable, and hence the TB piezoelectric model is an alternative theoretical framework for calculating electron-phonon interactions and PMF.

DOI: 10.1103/PhysRevB.98.125402

I. INTRODUCTION

Since its first observation in 1880, piezoelectricity has been one of the active topics in physics, materials, and engineering, because of its fascinating fundamental theory and wide applications in diverse fields. The striking features of piezoelectricity include the linear electromechanical coupling, reversibility, and robustness against perturbations. It is a fact that the piezoelectric polarization difference contains both electronic and ionic contributions, because of the ionic internal-strain induced by the macroscopic deformation as well. In a microscopic picture, the piezoelectricity contributed by ions is associated with the Born effective charges and the optoacoustic coupling in the context of lattice-dynamical theory; the electronic polarization difference in response to the strain (or stress) field and the electronic part of piezoelectric coefficient are correspondingly related to the Berry phase [1–3] and the first Chern form [4–6], which clarify the reason why piezoelectricity is robust like the topological quantum states [7,8]. Recently, the density functional theory (DFT) calculations [9–14], lattice dynamics calculations [15], and experiments [16–21] on the piezoelectricity of two-dimensional materials, particularly transition metal dichalcogenide monolayers (TMDMs) [9–12,15–18], group IV monochalcogenides [13], graphene [14,19], C₃N₄ [20], and α -In₂Se₃ [21], have shed new light on atomically thin piezotronics, flexible electronics, and optoelectronics.

TMDMs are semiconductors with experimentally tunable carrier mobilities [22] and a direct band gap [23], which

allows the field-effect transistors with a high on/off ratio [24]. The absence of inversion symmetry results in a spin-orbit coupling (SOC) which lifts the spin degeneracy [25], and the time-reversal symmetry keeps the valley degeneracy but makes the spin splitting at different valleys opposite [26]. The exotic spin-valley coupling together with the strong excitonic effect offers an avenue toward the valleytronics and optoelectronics [27]. The unique crystal structure and time-reversal symmetry are also responsible for the electromechanical couplings in TMDMs: (i) the trigonal prismatic structure with the main *d* orbital interactions of the transition metal atoms leads to the high stiffness and breaking strength [28], benefiting the nanomechanical resonators [29] and flexible devices [30]; (ii) the broken inversion symmetry renders the piezoelectricity [16,17]; (iii) the time-reversal symmetry enables the strain-induced valley-contrasting pseudomagnetic vector potentials [31–34], which measure the valley displacement analogous to that in strained graphene [35]; (iv) the lattice deformation modifies the electron-phonon interactions, which affect the electronic transport [36–38], optical properties [39], spin relaxation [40], and valley magnetization [41]. Although much progress on the piezoelectricity and strain effects on the phonon [42,43], electronic properties [44], optoelectronic properties [45], and work function [46] have been recently made by DFT and experiments, a microscopic theory, presenting the piezoelectric physics and revealing the correlation among these electromechanical couplings in TMDMs, is still lacking to date.

In this work we establish a microscopic piezoelectric theory using a combination of the tight-binding (TB) approach and Berry phase polarization theory, namely, TB piezoelectric theory. Using the linear feature of piezoelectricity and the correspondence between the TB piezoelectric model and the clamped-ion DFT model, we obtain the electronic Grüneisen

*wangyh49@mail.sysu.edu.cn

†wangbiao@mail.sysu.edu.cn

‡stsyl@mail.sysu.edu.cn

parameter (EGP), which characterizes the electron-phonon coupling in TMDMs. By virtue of the analytical piezoelectric model, we further explore the correlation between the electronic part of piezoelectric coefficient and strain-induced pseudomagnetic gauge field (PMF) and finally predict the PMF's values for strained TMDMs. The rest of this paper is organized into the following four sections. In Sec. II, we construct the TB piezoelectric theory for TMDMs. In Sec. III, the EGP measuring the electron-phonon couplings for TMDMs is calculated by the TB piezoelectric model. In Sec. IV, we build the analytical piezoelectric model in both of the first- and second-order continuum approximations and further predict the PMF for TMDMs by the analytical piezoelectric theory. Discussions on the experiments for the predicted EGP and PMF and conclusions are given in Sec. V.

II. TIGHT-BINDING PIEZOELECTRIC THEORY FOR TMDMs

A. Strain-dependent three-band TB Hamiltonian

TMDMs (MX_2 , $M = \text{Mo, W}$; $X = \text{S, Se, Te}$) have the general trigonal prismatic structure with its top view in Fig. 1(a), where the nearest-neighbor (NN), next-nearest-neighbor (NNN), and third-nearest-neighbor (TNN) lattice vectors \mathbf{r} are denoted by δ_i , χ_i , and $2\delta_i$, respectively, with $i = 1, \dots, 6$. For TMDMs, the conduction and valence bands near the Fermi energy are mainly contributed by d_{z^2} , d_{xy} , and $d_{x^2-y^2}$ orbitals of M atoms [47,48]. Consequently, their low-energy physics can be captured by the TB Hamiltonian including the NN, NNN, and TNN $d - d$ hoppings. In the real space, the TB Hamiltonian for unstrained TMDMs reads

$$\begin{aligned} H_0 = & \sum_{i,\zeta} \epsilon_\zeta c_{i,\zeta}^\dagger c_{i,\zeta} + \sum_{i,\delta} \sum_{\zeta,\zeta'} t_{\zeta,\zeta'} c_{i,\zeta}^\dagger c_{i+\delta,\zeta'} \\ & + \sum_{i,\chi} \sum_{\zeta,\zeta'} r_{\zeta,\zeta'} c_{i,\zeta}^\dagger c_{i+\chi,\zeta'} \\ & + \sum_{i,2\delta} \sum_{\zeta,\zeta'} u_{\zeta,\zeta'} c_{i,\zeta}^\dagger c_{i+2\delta,\zeta'}, \end{aligned} \quad (1)$$

where ϵ_ζ is the on-site energy, $c_{i,\zeta}^\dagger$ and $c_{i,\zeta}$ are the creation/annihilation operators for an electron with the orbital

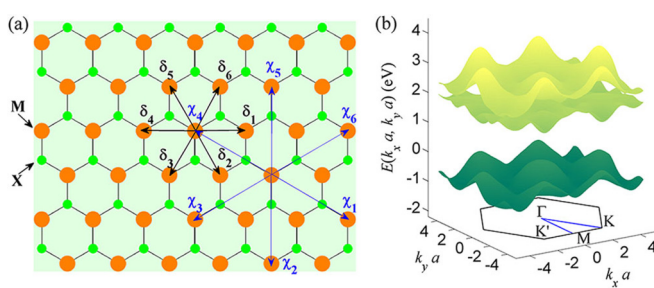


FIG. 1. (a) Top view of the trigonal prismatic structure for MX_2 with the lattice constant $a = |\delta_1|$ and the corresponding NN, NNN, and TNN lattice vectors δ_i , χ_i , and $2\delta_i$ for M atoms. (b) The three-band TB energy dispersion for MoS_2 with one negative valence band and two positive conduction bands, where the top of the valence band is shifted to zero, and the hexagon shows the first Brillouin zone (BZ).

ζ (d_{z^2} , d_{xy} or $d_{x^2-y^2}$) on site \mathbf{R}_i , δ , χ , and 2δ are the corresponding NN, NNN, and TNN lattice vectors as shown in Fig. 1(a), and $t_{\zeta,\zeta'}$, $r_{\zeta,\zeta'}$, and $u_{\zeta,\zeta'}$ are the corresponding hoppings. In general, the disorder effects on low-dimensional materials include two types. One is the local change of the on-site energy and the other is the changes of the electronic hoppings, owing to the changes of bond lengths and angles [49]. A typical example of the second type is the lattice deformation, where the strain enters into the Hamiltonian in the form of both scalar potential and effective magnetic vector potential. For the clamped ion models, it is assumed that the original lattice remains but the electronic hoppings are mainly modified by the changes of bond lengths [1,4–6,49]. In this way, the strain-modified hopping terms in the linear elastic approximation are written as $J_{\mathbf{r},\zeta-\zeta'}(\boldsymbol{\varepsilon}) = J_{\mathbf{r},\zeta-\zeta'}^0 [1 - (\beta_{ij}/|\mathbf{r}|^2) \sum_{mn} r_m \epsilon_{mn} r_n]$, where $\mathbf{r} = \mathbf{R}_j - \mathbf{R}_i$ are the lattice vectors pointed from i to j , $\epsilon_{mn} = (1/2)[\partial u_m / \partial r_n + \partial u_n / \partial r_m]$ is a component of the plane strain tensor for the in-plane intrinsic piezoelectricity under consideration, m and n denote x or y , J_r^0 denotes the initial hoppings for undeformed TMDMs in Table I, and the dimensionless EGP is defined as $\beta_{ij} = -[d \ln J_r(r^s)/d \ln r^s]|_{\boldsymbol{\varepsilon} \rightarrow 0}$ to measure how the electronic hopping changes with the strain-dependent length of \mathbf{r} , i.e., $r^s = |\mathbf{r}^s(\boldsymbol{\varepsilon})|$. Because the dominant hopping orbitals arise from all the d orbitals of M atoms [47], it is reasonable to approximately assume β_{ij} as a constant β .

Via the following Fourier transforms:

$$d_{i,\zeta} = \frac{1}{N} \sum_{\mathbf{k}} e^{i\mathbf{k}\cdot\mathbf{R}_i} d_{\mathbf{k},\zeta}, \quad d_{i,\zeta}^\dagger = \frac{1}{N} \sum_{\mathbf{k}} e^{-i\mathbf{k}\cdot\mathbf{R}_i} d_{\mathbf{k},\zeta}^\dagger, \quad (2)$$

we further write the strain-dependent TB Hamiltonian in momentum space as

$$H(\boldsymbol{\varepsilon}) = \sum_{\mathbf{k}} [d_{\mathbf{k},z^2}^\dagger \quad d_{\mathbf{k},xy}^\dagger \quad d_{\mathbf{k},x^2-y^2}^\dagger] H(\mathbf{k}, \boldsymbol{\varepsilon}) \begin{bmatrix} d_{\mathbf{k},z^2} \\ d_{\mathbf{k},xy} \\ d_{\mathbf{k},x^2-y^2} \end{bmatrix}. \quad (3)$$

The Hamiltonian $H(\mathbf{k}, \boldsymbol{\varepsilon})$ consists of the NN (δ), NNN (χ), and TNN (2δ) components, i.e.,

$$H(\mathbf{k}, \boldsymbol{\varepsilon}) = H_\delta(\mathbf{k}, \boldsymbol{\varepsilon}) + H_\chi(\mathbf{k}, \boldsymbol{\varepsilon}) + H_{2\delta}(\mathbf{k}, \boldsymbol{\varepsilon}). \quad (4)$$

The matrix elements for $H_\delta^{i,j}(\mathbf{k}, \boldsymbol{\varepsilon})$, $H_\chi^{i,j}(\mathbf{k}, \boldsymbol{\varepsilon})$, and $H_{2\delta}^{i,j}(\mathbf{k}, \boldsymbol{\varepsilon})$ with $(i = 1, 2, 3; j \geq i)$ read

$$H_\delta^{i,j}(\mathbf{k}, \boldsymbol{\varepsilon}) = \sum_{l=1}^6 J_{\delta_{il}, \zeta_i - \zeta_j}(\boldsymbol{\varepsilon}) e^{i\mathbf{k}\cdot\delta_l} + \epsilon_i \delta_{ij}, \quad (5a)$$

$$H_\chi^{i,j}(\mathbf{k}, \boldsymbol{\varepsilon}) = \sum_{l=1}^6 J_{\chi_{il}, \zeta_i - \zeta_j}(\boldsymbol{\varepsilon}) e^{i\mathbf{k}\cdot\chi_l}, \quad (5b)$$

$$H_{2\delta}^{i,j}(\mathbf{k}, \boldsymbol{\varepsilon}) = \sum_{l=1}^6 J_{2\delta_{il}, \zeta_i - \zeta_j}(\boldsymbol{\varepsilon}) e^{i\mathbf{k}\cdot2\delta_l}, \quad (5c)$$

where ϵ_1 , ϵ_2 , and ϵ_3 ($\epsilon_3 = \epsilon_2$) are the on-site energy, δ_{ij} is the Kronecker delta, and ζ_i and ζ_j denote the d

TABLE I. Hoppings between different d orbitals of M atoms for MX_2 . The first row shows the combinations of arbitrary two d orbitals, the first column displays the NN, NNN, and TNN lattice vectors, and the other columns show their corresponding hoppings for different lattice vectors. The values of these TB parameters are listed in Table III of Ref. [47].

	$d_{z^2} - d_{z^2}$	$d_{xy} - d_{xy}$	$d_{x^2-y^2} - d_{x^2-y^2}$	$d_{z^2} - d_{xy}$	$d_{z^2} - d_{x^2-y^2}$	$d_{xy} - d_{x^2-y^2}$
δ_1	t_0	t_{11}	t_{22}	t_1	t_2	t_{12}
δ_2	t_0	$\frac{t_{11}+3t_{22}}{4}$	$\frac{3t_{11}+t_{22}}{4}$	$\frac{t_1-\sqrt{3}t_2}{2}$	$-\frac{t_2+\sqrt{3}t_1}{2}$	$\frac{\sqrt{3}(t_{22}-t_{11})}{4} - t_{12}$
δ_3	t_0	$\frac{t_{11}+3t_{22}}{4}$	$\frac{3t_{11}+t_{22}}{4}$	$-\frac{t_1-\sqrt{3}t_2}{2}$	$-\frac{t_2+\sqrt{3}t_1}{2}$	$\frac{\sqrt{3}(t_{11}-t_{22})}{4} + t_{12}$
δ_4	t_0	t_{11}	t_{22}	$-t_1$	t_2	$-t_{12}$
δ_5	t_0	$\frac{t_{11}+3t_{22}}{4}$	$\frac{3t_{11}+t_{22}}{4}$	$-\frac{t_1+\sqrt{3}t_2}{2}$	$-\frac{t_2-\sqrt{3}t_1}{2}$	$\frac{\sqrt{3}(t_{22}-t_{11})}{4} + t_{12}$
δ_6	t_0	$\frac{t_{11}+3t_{22}}{4}$	$\frac{3t_{11}+t_{22}}{4}$	$\frac{t_1+\sqrt{3}t_2}{2}$	$-\frac{t_2-\sqrt{3}t_1}{2}$	$\frac{\sqrt{3}(t_{11}-t_{22})}{4} - t_{12}$
χ_1	r_0	r_{11}	$\frac{\sqrt{3}r_{11}+2r_{12}}{\sqrt{3}}$	r_1	$-\frac{r_1}{\sqrt{3}}$	r_{12}
χ_2	r_0	$r_{11} + \sqrt{3}r_{12}$	$\frac{\sqrt{3}r_{11}-r_{12}}{\sqrt{3}}$	0	$\frac{2r_2}{\sqrt{3}}$	0
χ_3	r_0	r_{11}	$\frac{\sqrt{3}r_{11}+2r_{12}}{\sqrt{3}}$	$-r_1$	$-\frac{r_1}{\sqrt{3}}$	$-r_{12}$
χ_4	r_0	r_{11}	$\frac{\sqrt{3}r_{11}+2r_{12}}{\sqrt{3}}$	r_2	$-\frac{r_2}{\sqrt{3}}$	r_{12}
χ_5	r_0	$r_{11} + \sqrt{3}r_{12}$	$\frac{\sqrt{3}r_{11}-r_{12}}{\sqrt{3}}$	0	$\frac{2r_1}{\sqrt{3}}$	0
χ_6	r_0	r_{11}	$\frac{\sqrt{3}r_{11}+2r_{12}}{\sqrt{3}}$	$-r_2$	$-\frac{r_2}{\sqrt{3}}$	$-r_{12}$
$2\delta_1$	u_0	u_{11}	u_{22}	u_1	u_2	u_{12}
$2\delta_2$	u_0	$\frac{u_{11}+3u_{22}}{4}$	$\frac{3u_{11}+u_{22}}{4}$	$\frac{u_1-\sqrt{3}u_2}{2}$	$-\frac{u_2+\sqrt{3}u_1}{2}$	$\frac{\sqrt{3}(u_{22}-u_{11})}{4} - u_{12}$
$2\delta_3$	u_0	$\frac{u_{11}+3u_{22}}{4}$	$\frac{3u_{11}+u_{22}}{4}$	$-\frac{u_1-\sqrt{3}u_2}{2}$	$-\frac{u_2+\sqrt{3}u_1}{2}$	$\frac{\sqrt{3}(u_{11}-u_{22})}{4} + u_{12}$
$2\delta_4$	u_0	u_{11}	u_{22}	$-u_1$	u_2	$-u_{12}$
$2\delta_5$	u_0	$\frac{u_{11}+3u_{22}}{4}$	$\frac{3u_{11}+u_{22}}{4}$	$-\frac{u_1+\sqrt{3}u_2}{2}$	$-\frac{u_2-\sqrt{3}u_1}{2}$	$\frac{\sqrt{3}(u_{22}-u_{11})}{4} + u_{12}$
$2\delta_6$	u_0	$\frac{u_{11}+3u_{22}}{4}$	$\frac{3u_{11}+u_{22}}{4}$	$\frac{u_1+\sqrt{3}u_2}{2}$	$-\frac{u_2-\sqrt{3}u_1}{2}$	$\frac{\sqrt{3}(u_{11}-u_{22})}{4} - u_{12}$

orbitals in Table I. The obtained strain-dependent Hamiltonian $H(\mathbf{k}, \boldsymbol{\varepsilon})$ in Eqs. (4) and (5) can be used to calculate the piezoelectric Berry curvature $\Omega_{i,jk}$ such that the electronic part of piezoelectric coefficients can be further evaluated.

B. Electronic contribution to piezoelectric coefficients

Under a time-dependent nonelectromagnetic perturbation with a slow variation, the semiclassical dynamical equation for the n th energy band reads $\dot{r}_n = [\partial E_n^0(\mathbf{k})/\partial(\hbar\mathbf{k})] - \Omega_{\mathbf{k},t}^n$, and $\mathbf{k} = 0$, where $E_n^0(\mathbf{k})$ is the energy for the system without perturbations and $\Omega_{\mathbf{k},t}^n$ is the Berry curvature with respect to \mathbf{k} and t . The perturbation-induced adiabatic charge current in 2D systems reads $j(t) = 2e \sum_n \int_{BZ} \Omega_{\mathbf{k},t}^n d\mathbf{k}/(2\pi)^2$. For piezoelectricity, the adiabatic process varies from the initial state with $\boldsymbol{\varepsilon}(0) = \mathbf{0}$ to the final state with $\boldsymbol{\varepsilon}(T) = \boldsymbol{\varepsilon}$, i.e., $\boldsymbol{\varepsilon}(T) = \Delta\boldsymbol{\varepsilon}$, owing to $\boldsymbol{\varepsilon} - \mathbf{0} = \Delta\boldsymbol{\varepsilon}$. Then, the piezoelectric adiabatic current is $j(t) = 2e \sum_{jk} \sum_n \int_{BZ} \Omega_{\mathbf{k},\varepsilon_{jk}}^n \dot{\varepsilon}_{jk} d\mathbf{k}/(2\pi)^2$. The continuity equation and the relation between polarization and charge densities require the polarization difference along the i direction to satisfy $\Delta P_i = \int_0^T j_i(t) dt$, i.e.,

$$\Delta P_i = \sum_{jk} \left(2e \sum_n \int_{BZ} \Omega_{\mathbf{k}_i, \varepsilon_{jk}}^n d\mathbf{k}/(2\pi)^2 \right) \Delta \varepsilon_{jk}. \quad (6)$$

Therefore, the electronic part of piezoelectric coefficient e_{ijk} for TMDMs, i.e., $e_{ijk} = (\partial P_i / \partial \varepsilon_{jk})|_{\boldsymbol{\varepsilon} \rightarrow \mathbf{0}}$, reads

$$e_{ijk} = \frac{e}{2\pi^2} \int_{BZ} \Omega_{i,jk} d\mathbf{k}, \quad (7a)$$

$$\Omega_{i,jk} = i \sum_{m=1}^2 \frac{\langle u_v^0 | v_i | u_{cm}^0 \rangle \langle u_{cm}^0 | w_{jk} | u_v^0 \rangle - \text{c.c.}}{(E_v^0 - E_{cm}^0)^2}, \quad (7b)$$

where $\Omega_{i,jk}$ is a short-hand notation of $\Omega_{\mathbf{k}_i, \varepsilon_{jk}}|_{\boldsymbol{\varepsilon} \rightarrow \mathbf{0}}$, $E_v^0(E_c^0)$ and $u_v^0(u_{cm}^0)$ are the corresponding eigenvalues and normalized eigenstates with one valence (v) band and two conduction (c) bands for the unstrained TMDMs, as shown in Fig. 1(b), $v_i = \partial[H(\mathbf{k}, \boldsymbol{\varepsilon})|_{\boldsymbol{\varepsilon} \rightarrow \mathbf{0}}]/\partial k_i$, $w_{jk} = \partial H(\mathbf{k}, \boldsymbol{\varepsilon})/\partial \varepsilon_{jk}$, and c.c. denotes the complex conjugate.

Let us use the TB piezoelectric model to calculate both the piezoelectric Berry curvature and piezoelectric coefficients for MoS₂, as an example of TMDMs because of their similarity. We adopt the TB parameters in Table III of Ref. [47] and $\beta = 2$ [50]. Considering $\varepsilon_{12} = \varepsilon_{21}$, we have $e_{112} = e_{121}$ and $e_{212} = e_{221}$. Therefore, only six piezoelectric coefficients need to be calculated. Figure 2 shows the distributions of the piezoelectric Berry curvature $\Omega_{i,jk}$ for MoS₂ in momentum space. It can be seen that $\Omega_{1,11}$, $\Omega_{1,22}$, and $\Omega_{2,12}$ are odd functions of k_x and k_y inside the BZ in Figs. 2(a), 2(c), and 2(e), respectively. Consequently, corresponding piezoelectric coefficients, e_{111} , e_{122} , e_{212} , and e_{221} , as their integrals over the BZ, must be zero. The other $\Omega_{1,12}$, $\Omega_{2,11}$, and $\Omega_{2,22}$ are even functions of

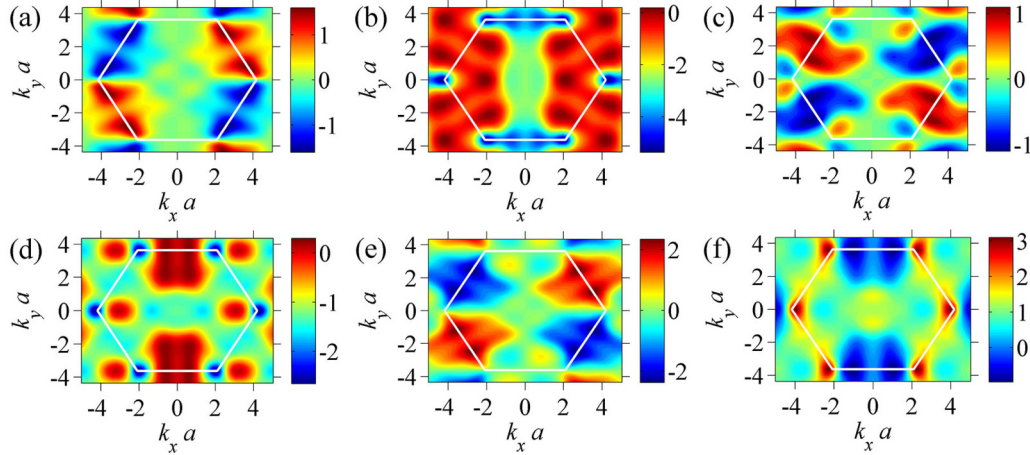


FIG. 2. Contour maps of piezoelectric Berry curvature (in units of Å) as a function of $k_x a$ and $k_y a$ in momentum space for MoS₂: (a) $\Omega_{1,11}$, (b) $\Omega_{1,12}$, (c) $\Omega_{1,22}$, (d) $\Omega_{2,11}$, (e) $\Omega_{2,12}$, and (f) $\Omega_{2,22}$. The white hexagons show the BZ.

k_x and k_y inside the BZ in Figs. 2(b), 2(d), and 2(f), respectively, and hence e_{112} , e_{211} , and e_{222} are nonzero. The values of these piezoelectric coefficients are listed in Table II. In general, the D_{3h} point group requires $e_{111} = e_{122} = e_{212} = e_{221} = 0$ and $e_{211} = -e_{222} = e_{112}/2 = e_{121}/2$, if the piezoelectric coefficient is defined as $e_{ijk} = (\partial P_i / \partial \varepsilon_{jk})|_{\varepsilon \rightarrow 0}$, with $\varepsilon_{jk} = (1/2)[\partial u_j / \partial r_k + \partial u_k / \partial r_j]$ [5]. The results in Table II obey the symmetry of D_{3h} and agree well with both DFT [9] and experiments [17]. It should be noticed that the experimental result is corresponding to the relaxed-ion piezoelectric coefficient contributed by both electrons and ions. In Table II, the clamped-ion TB result is approximately comparable to the experiment, because the electronic contribution is much larger than the ionic part for MoS₂ and WS₂ [9,15], but note that the comparison for other TMDMs is inappropriate.

III. ELECTRON-PHONON INTERACTIONS AND EGP

In the first order approximation of the atomic displacements, the electron-phonon coupling Hamiltonian H_{ep} reads [51]

$$H_{ep} = \frac{1}{\sqrt{A}} \sum_{k,p;k',p';q,v} g_{k,p;k',p';q,v}^v c_{k,p}^\dagger c_{k',p'} \phi_{q,v}, \quad (8)$$

where A is the area, $\phi_{q,v} = \sqrt{\hbar \omega_{q,v}} / 2(b_{q,v} + b_{-q,v}^\dagger)$ is the phonon operator with its wave vector q , k and k' are the electron wave vectors, and p and p' are the energy band indexes. The electron-phonon matrix element $g_{k,p;k',p'}^v$ in the

TB approximation reads

$$g_{k,p;k',p'}^v = \frac{\sum_{n',s,s'} U_{s,p}^*(\mathbf{k}) U_{s',p'}(\mathbf{k}') \mathbf{O} \cdot \nabla J(0, s; n', s')|_0}{\sqrt{\mu \omega_{k-k',v}}}, \quad (9)$$

where μ is the mass per unit area, U is the unitary matrix that diagonalizes the strain-independent $H(\mathbf{k}, \varepsilon)|_{\varepsilon \rightarrow 0}$, $\mathbf{O} = e^{ik' \cdot \mathbf{R}_{n'}} S_s^v(\mathbf{k} - \mathbf{k}') - e^{i\mathbf{k} \cdot \mathbf{R}_n} S_{s'}^v(\mathbf{k} - \mathbf{k}')$ with the phonon polarization vector S_s^v , and $J(0, s; n', s')$ is the matrix element of the NN interactions between atoms $(0, s)$ and (n', s') [52]. Using $\beta = -[d \ln J_r(r^s) / d \ln r^s]|_{\varepsilon \rightarrow 0}$, we have $\nabla J(0, s; n', s')|_0 \cdot \hat{r} = \beta J_r^0 / r$, with the NN unit vector \hat{r} and length r of \mathbf{r} . Owing to $|g_{k,p;k',p'}^v| \propto \beta$, consequently, EGP is usually used to characterize the electron-phonon coupling within the TB framework [31–33,35,52].

EGP is important to determine the electron-phonon coupling, PMF [31–34], and strain-modulated electronic transports in 2D materials [49,53,54]. Therefore, it is meaningful to predict EGP of TMDMs. The strain-modulated $H(\mathbf{k}, \varepsilon)$ and Eqs. (7) show that e_{ijk} is proportional to EGP (β), i.e., $e_{ijk} \propto \beta$. Therefore, if the clamped-ion piezoelectric coefficient has been obtained from DFT, one can inversely determine EGP, i.e., $\beta/\beta_0 = e_{ijk}/e_{ijk}^0$, where e_{ijk}^0 is a calculated reference value of the TB piezoelectric coefficient for $\beta_0 = 1$ by Eqs. (7), according to the consistency between the TB piezoelectric model and DFT results. The obtained results in Table III show that β for Mo-based TMDMs is about 2. In addition, β for Mo-based TMDMs is larger than that for W-based TMDMs. It means that the electronic hoppings for Mo 4d orbitals change faster with the bond length than those

TABLE II. Obtained piezoelectric coefficients (10^{-10} C/m) of MoS₂ from the TB piezoelectric theory. Expt. denotes the experimental values.

	e_{111}	e_{122}	e_{212}	e_{112}	e_{211}	e_{222}
TB	0	0	0	-5.83	-2.89	2.87
DFT [9]					3.06	
Expt. [17]					2.9 ± 0.5	

TABLE III. EGP (β) for TMDMs. e_{222}^0 (10^{-10} C/m) is a calculated reference value for $\beta_0 = 1$ by Eqs. (7).

	MoS ₂	MoSe ₂	MoTe ₂	WS ₂	WSe ₂	WTe ₂
e_{222} [9]	3.06	2.80	2.98	2.20	1.93	1.60
e_{222}^0	1.4365	1.4057	1.3672	1.4450	1.4560	1.4002
$\beta = e_{222}/e_{222}^0$	2.13	1.99	2.18	1.52	1.33	1.14

for W 5d orbitals. Because the distribution of W 5d orbitals in space is wider than that of Mo 4d orbitals, the interaction among W 5d orbitals is more robust against the strain than that of Mo 4d orbitals.

IV. ANALYTICAL PIEZOELECTRIC MODEL AND PMF FOR TMDMS

A. Strain-dependent $k \cdot p$ Hamiltonian and pseudomagnetic vector potential

Expanding the three-band Hamiltonian $H(\mathbf{k}, \boldsymbol{\varepsilon})$ at the K valley and using the Löwdin partitioning method [55], we write the strain-dependent $k \cdot p$ Hamiltonian as

$$H_K(\mathbf{q}, \boldsymbol{\varepsilon}) = H_0^1(\mathbf{q}) + H_0^2(\mathbf{q}) + H_S^s(\boldsymbol{\varepsilon}) + H_S^v(\boldsymbol{\varepsilon}), \quad (10a)$$

$$H_0^1(\mathbf{q}) = \begin{bmatrix} \Delta/2 & at(q_x - iq_y) \\ at(q_x + iq_y) & -\Delta/2 \end{bmatrix}, \quad (10b)$$

$$H_0^2(\mathbf{q}) = \begin{bmatrix} \gamma_1 a^2 (q_x^2 + q_y^2) & \gamma_3 a^2 (q_x + iq_y)^2 \\ \gamma_3 a^2 (q_x - iq_y)^2 & \gamma_2 a^2 (q_x^2 + q_y^2) \end{bmatrix}, \quad (10c)$$

$$H_S^s(\boldsymbol{\varepsilon}) = \begin{bmatrix} \alpha_c \beta (\varepsilon_{xx} + \varepsilon_{yy}) & 0 \\ 0 & \alpha_v \beta (\varepsilon_{xx} + \varepsilon_{yy}) \end{bmatrix}, \quad (10d)$$

$$H_S^v(\boldsymbol{\varepsilon}) = \alpha \beta \begin{bmatrix} 0 & \varepsilon_{xx} - \varepsilon_{yy} - i2\varepsilon_{xy} \\ \varepsilon_{xx} - \varepsilon_{yy} + i2\varepsilon_{xy} & 0 \end{bmatrix}, \quad (10e)$$

where the first term $H_0^1(\mathbf{q})$ is the first order approximation, i.e., the gapped Dirac Hamiltonian [56], the second term is the trigonal warping [57], and the strain perturbation contains the third and fourth terms, i.e., the strain-induced scalar potential (V_c and V_v) and pseudomagnetic vector potential (\mathbf{A}), with their corresponding forms as follows:

$$V_{c(v)} = \alpha_{c(v)} \beta (\varepsilon_{xx} + \varepsilon_{yy}), \quad (11a)$$

$$A_x = \frac{\hbar \alpha \beta}{aet} (\varepsilon_{xx} - \varepsilon_{yy}), \quad A_y = \frac{\hbar \alpha \beta}{aet} (-2\varepsilon_{xy}). \quad (11b)$$

The obtained scalar and vector potentials in the linear elastic approximation have the similar forms as those for other 2D hexagonal crystals such as h -BN and graphene [54,58–63], but with different β (see Sec. III). All these energy parameters (Δ , t , γ_1 , γ_2 , and γ_3) in the nonperturbative terms can be obtained by the fitting between the TB and $k \cdot p$ models for unstrained TMDMs. The other energy parameters (α_c , α_v , and α) in the strain perturbation terms in principle can also be obtained through the energy band comparison between the DFT and TB calculations for strained TMDMs. In addition, the pseudomagnetic vector potential \mathbf{A} is direction dependent. If the x direction has an angle θ with respect to the armchair direction of TMDMs, \mathbf{A} has the following general forms [64–70]:

$$A_x = \frac{\hbar \alpha \beta}{aet} [(\varepsilon_{xx} - \varepsilon_{yy}) \cos(3\theta) - 2\varepsilon_{xy} \sin(3\theta)], \quad (12a)$$

$$A_y = -\frac{\hbar \alpha \beta}{aet} [(\varepsilon_{xx} - \varepsilon_{yy}) \sin(3\theta) + 2\varepsilon_{xy} \cos(3\theta)]. \quad (12b)$$

TABLE IV. PMF strength B_0 (10^{-5} T m) for TMDMs. The energy parameters t and Δ (in units of eV) are obtained from the fitting between the first order continuum approximation and the TB model.

	MoS ₂	MoSe ₂	MoTe ₂	WS ₂	WSe ₂	WTe ₂
t	1.0799	0.8984	0.7213	1.3315	1.1395	0.9739
Δ	1.6579	1.4293	1.2302	1.8062	1.5412	1.0668
B_0	5.4416	5.0429	5.51	3.7576	3.2935	2.5795

B. Analytical piezoelectric model

As shown in Fig. 2(f), the Berry curvature $\Omega_{2,22}$ is mainly located in the six corners of the BZ. This means that e_{222} is mainly contributed by the Berry curvatures in the vicinity of $K(K')$ point. Therefore, it is effective to analytically evaluate e_{222} by both the strain-dependent $k \cdot p$ Hamiltonian in Eqs. (10) and the piezoelectric coefficients in Eqs. (7). Because the SOC splitting is much less than the band gap in TMDMs [47,48], SOC has a weak influence on the piezoelectricity. In addition, the time-reversal invariant allows us to consider the piezoelectricity only at the K valley, because of the valley degeneracy. We first consider the piezoelectricity based on the first order $k \cdot p$ Hamiltonian and then explore the trigonal warping effects on the piezoelectricity. The fitted energy parameters t and Δ in the first order approximation are listed in Table IV. In order to evaluate the piezoelectric Berry curvatures in the first order approximation (neglecting the trigonal warping), we need to first acquire the energy eigenvalues and normalized eigenstates for the conduction (+) and valence (−) bands of TMDMs without the strain perturbation, as follows:

$$E_{\pm}^0 = \pm \sqrt{a^2 t^2 (q_x^2 + q_y^2) + (\Delta/2)^2}, \quad (13a)$$

$$|u_{\pm}^0\rangle = \frac{1}{\sqrt{2E_{\pm}^0}} \begin{bmatrix} \frac{at(q_x - iq_y)}{\sqrt{E_{\pm}^0 \mp (\Delta/2)}} \\ \pm \sqrt{E_{\pm}^0 \mp (\Delta/2)} \end{bmatrix}. \quad (13b)$$

Then the partial derivatives of Hamiltonian (neglecting the trigonal warping) in Eqs. (10) with respect to q_y and ε_{yy} read

$$\frac{\partial H_0(\mathbf{q})}{\partial q_y} = \frac{\partial H_0^1(\mathbf{q})}{\partial q_y} = \begin{pmatrix} 0 & -iat \\ iat & 0 \end{pmatrix}, \quad (14a)$$

$$\frac{\partial H_K(\mathbf{q}, \boldsymbol{\varepsilon})}{\partial \varepsilon_{yy}} = \frac{\partial H_S^s(\boldsymbol{\varepsilon})}{\partial \varepsilon_{yy}} + \frac{\partial H_S^v(\boldsymbol{\varepsilon})}{\partial \varepsilon_{yy}}, \quad (14b)$$

$$\frac{\partial H_S^s(\boldsymbol{\varepsilon})}{\partial \varepsilon_{yy}} = \begin{pmatrix} \alpha_c \beta & 0 \\ 0 & \alpha_v \beta \end{pmatrix}, \quad (14c)$$

$$\frac{\partial H_S^v(\boldsymbol{\varepsilon})}{\partial \varepsilon_{yy}} = \begin{pmatrix} 0 & -\alpha \beta \\ -\alpha \beta & 0 \end{pmatrix}. \quad (14d)$$

Inserting Eqs. (14) into the Berry curvature expression Eq. (7), we obtain the piezoelectric Berry curvatures $\Omega_{2,22}^s$ and $\Omega_{2,22}^v$ contributed by the corresponding scalar and vector potentials, as follows:

$$\Omega_{2,22}^s = \frac{a^2 t^2 (\alpha_c - \alpha_v) \beta q_x}{4[a^2 t^2 (q_x^2 + q_y^2) + (\Delta/2)^2]^{3/2}}, \quad (15a)$$

$$\Omega_{2,22}^v = \frac{at\alpha\beta\Delta}{4[a^2t^2(q_x^2 + q_y^2) + (\Delta/2)^2]^{3/2}}, \quad (15b)$$

where α_c and α_v are the energy parameters of conduction and valence bands for the scalar potential, respectively, and α is the energy parameter for the vector potential. Then the piezoelectric coefficient reads

$$\begin{aligned} e_{222} &= \frac{4e}{(2\pi)^2} \int_0^{2\pi} d\theta \int_0^{q_m} (\Omega_{2,22}^s + \Omega_{2,22}^v) q dq \\ &= \frac{e\alpha\beta}{\pi at} \left(1 - \frac{\sqrt{3}\Delta}{\sqrt{16\sqrt{3}\pi t^2 + 3\Delta^2}} \right), \end{aligned} \quad (16)$$

where the factor 4 contains both the spin and valley degenerates, $q = \sqrt{q_x^2 + q_y^2}$, and $\pi q_m^2 = S_{BZ}/2$ with the first BZ area S_{BZ} ($8\pi^2/\sqrt{3}a^2$). Equation (15a) shows that $\Omega_{2,22}^s$ is an odd function of q_x . Therefore, $\Omega_{2,22}^s$ affects the work function [46] but has no contributions to piezoelectricity, because its integral is zero. Consequently, $\Omega_{2,22}^v$ mainly contributes to e_{222} . The analytical expression of e_{222} in Eq. (16) demonstrates the clear relation among the piezoelectricity, lattice constant, band gap, EGP, and energy parameters (t and α), and hence it provides a direct estimation of the piezoelectric coefficient for TMDMs.

C. Electromechanical coupling correlations between PMF and piezoelectricity

For a deformation without strain gradients, there is no strain-induced PMF in 2D materials. In addition, the lattice correction has no contributions to PMF. In general, if the armchair direction of TMDMs has an angle θ to the x axis, the PMF, $B = (\nabla \times A) \cdot \mathbf{e}_z$, is written as [64–70]

$$\begin{aligned} \frac{B}{B_0} &= - \left[\frac{\partial(\varepsilon_{xx} - \varepsilon_{yy})}{\partial x} - 2 \frac{\partial\varepsilon_{xy}}{\partial y} \right] \sin(3\theta) \\ &\quad - \left[\frac{\partial(\varepsilon_{xx} - \varepsilon_{yy})}{\partial y} + 2 \frac{\partial\varepsilon_{xy}}{\partial x} \right] \cos(3\theta), \end{aligned} \quad (17)$$

where $B_0 = \hbar\alpha\beta/aet$ represents the PMF strength. Using Eq. (16) and $B_0 = \hbar\alpha\beta/aet$, we cancel the unknown factor $\alpha\beta$ and further write the PMF strength as

$$B_0 = \frac{\pi\hbar\sqrt{16\sqrt{3}\pi t^2 + 3\Delta^2}}{e^2(\sqrt{16\sqrt{3}\pi t^2 + 3\Delta^2} - \sqrt{3}\Delta)} e_{222}. \quad (18)$$

The calculated B_0 for TMDMs by Eq. (18) is listed in Table IV. For the same deformation B_0 for TMDMs is larger than that for graphene with its PMF strength ($B_0 \sim 1 \times 10^{-5}$ T m) [35]. The strain-induced large PMF in TMDMs is manifested by the giant valley drift [71]. Therefore, strain even with a small magnitude has a remarkable effect on the electronic, optical, and magnetic properties of TMDMs [41,44–46].

D. Trigonal warping effects on the piezoelectricity of TMDMs

The trigonal warping changes the distribution of the Berry curvatures in the first order continuum approximation near

TABLE V. Fitting values for energy parameters Δ , t , γ_1 , γ_2 , and γ_3 (in units of eV) between the continuum approximation involving the trigonal warping and the TB model for TMDMs.

	MoS ₂	MoSe ₂	MoTe ₂	WS ₂	WSe ₂	WTe ₂
Δ	1.6579	1.4293	1.2302	1.8062	1.5412	1.0668
t	1.0301	0.8752	0.7186	1.2910	1.0812	0.9462
γ_1	0.1413	0.0803	0.1349	0.1783	0.1802	0.1903
γ_2	0.0115	0.0203	0.0282	0.0531	0.0086	0.0857
γ_3	-0.1047	-0.0826	-0.0138	-0.0853	-0.0760	-0.0692

the K valley and hence also contributes to the piezoelectricity of TMDMs. By fitting the energy band structures between the TB and $\mathbf{k} \cdot \mathbf{p}$ models for unstrained TMDMs, we obtain the energy parameters (Δ , t , γ_1 , γ_2 , and γ_3) for all TMDMs involving the second order approximations, as shown in Table V. For the second order approximation, the energy eigenvalues and normalized eigenstates in Eqs. (10) for the conduction (+) and valence (-) bands read

$$E_{\pm}^0 = \frac{\Delta_{+} + \Delta_{-} \pm \sqrt{4|f(q_x, q_y)|^2 + (\Delta_{+} - \Delta_{-})^2}}{2}, \quad (19a)$$

$$|u_{\pm}^0\rangle = \frac{1}{\sqrt{2E_{+}^0 - \Delta_{+} - \Delta_{-}}} \begin{bmatrix} \frac{f(q_x, q_y)}{\sqrt{E_{+}^0 - \Delta_{\pm}}} \\ \pm \sqrt{E_{+}^0 - \Delta_{\pm}} \end{bmatrix}, \quad (19b)$$

where Δ_{+} , Δ_{-} , and $f(q_x, q_y)$ have been set as

$$\Delta_{+} = \gamma_1 a^2 (q_x^2 + q_y^2) + (\Delta/2), \quad (20a)$$

$$\Delta_{-} = \gamma_2 a^2 (q_x^2 + q_y^2) - (\Delta/2), \quad (20b)$$

$$f(q_x, q_y) = at(q_x - iq_y) + \gamma_3 a^2 (q_x + iq_y)^2. \quad (20c)$$

The partial derivative of Hamiltonian including the trigonal warping in Eqs. (10) with respect to q_y reads

$$\frac{\partial H_0(\mathbf{q})}{\partial q_y} = \begin{pmatrix} 2\gamma_1 a^2 q_y & \partial f(q_x, q_y)/\partial q_y \\ \partial f^*(q_x, q_y)/\partial q_y & 2\gamma_2 a^2 q_y \end{pmatrix}, \quad (21)$$

where $\partial f(q_x, q_y)/\partial q_y = -iat + i2\gamma_3 a^2 (q_x + iq_y)$ and $\partial f^*(q_x, q_y)/\partial q_y = iat - i2\gamma_3 a^2 (q_x - iq_y)$. In this case, the corresponding Berry curvatures read

$$\Omega_{2,22} = \Omega_{2,22}^s + \Omega_{2,22}^v, \quad (22a)$$

$$\Omega_{2,22}^s = \frac{2a\beta(\alpha_c - \alpha_v)(t - 2aq_x\gamma_3)(aq_x t + a^2 q^2 \gamma_3)}{[4|f(q_x, q_y)|^2 + (\Delta_{+} - \Delta_{-})^2]^{3/2}}, \quad (22b)$$

$$\Omega_{2,22}^v = \frac{2a\alpha\beta(t - 2aq_x\gamma_3)[2a^2 q_y^2 (\gamma_2 - \gamma_1) + (\Delta_{+} - \Delta_{-})]}{[4|f(q_x, q_y)|^2 + (\Delta_{+} - \Delta_{-})^2]^{3/2}}. \quad (22c)$$

Then the piezoelectric coefficient e_{222} reads

$$e_{222} = \frac{4e}{(2\pi)^2} \int_0^{2\pi} d\theta \int_0^{q_m} (\Omega_{2,22}^s + \Omega_{2,22}^v) q dq, \quad (23)$$

where $q = \sqrt{q_x^2 + q_y^2}$, and $\pi q_m^2 = S_{BZ}/2$ with $S_{BZ} = 8\pi^2/\sqrt{3}a^2$ in order to conserve the total number of states. Different from the first order approximation, the strain-induced

scalar potential in the second approximation also benefits the piezoelectric coefficient, because the previous odd distribution of the Berry curvature $\Omega_{2,22}^2$ in Eq. (15a) with respect to q_x has been changed by the trigonal warping, as demonstrated in Eqs. (22b). Consequently, the piezoelectric coefficient contains two parts contributed by both scalar and vector potentials.

V. DISCUSSIONS AND CONCLUSIONS

We now briefly comment on the experiments for the predicted EGP and PMF by the TB piezoelectric theory and then make conclusions. Although the phonon Grüneisen parameter can be extracted from the Raman spectroscopy [42,72], it is challenging to experimentally measure EGP (β). Recently, the time- and angle-resolved photoemission spectroscopy (tr-ARPES) has been extended to map momentum-resolved electronic structure and electron-phonon interaction [73]. Therefore, the strain-tunable electronic band structure and electron-phonon coupling [38] for TMDMs can be mapped by tr-ARPES such that β is determined, similar to that of a carbon nanotube [74]. The strain gradient induced by the nanobubbles [75] or a uniaxial stretch [76] induces PMF, which leads to pseudomagnetic quantum Hall effect [77]. Consequently, the scanning tunneling microscopy and spectroscopy are used to measure the PMF [78].

We develop an atomic-scale TB piezoelectric theory for TMDMs. By means of the consistency between the TB and clamped-ion DFT piezoelectric models, we predict the values of EGP for TMDMs. Using the TB piezoelectric model in the continuum approximation, we further build the electromechanical coupling correlation between the electronic part of piezoelectric coefficient and strain-induced PMF and also forecast the values of PMF for TMDMs. Our results will spark more interest in electromechanical couplings in 2D materials and benefit novel atomically thin piezotronics and straintronics.

Note added. We note two recent studies [6,79]. In Ref. [6], they obtain the piezoelectric coefficients for some of the TMDMs in the continuum approximation. In Ref. [79], the TB Hamiltonian for 2D strained hexagonal crystals is also constructed.

ACKNOWLEDGMENTS

This work was supported financially by National Natural Science Foundation of China under Grants No. 11502308, No. 11832019, No. 11232015, and No. 11572355, Guangdong Natural Science Foundation of China under Grant No. 2016A030310205, and the fundamental research funds for the central universities under Grant No. 17lgpy31.

Y.W. and Z.W. contributed equally to this work.

-
- [1] R. D. King-Smith and D. Vanderbilt, *Phys. Rev. B* **47**, 1651 (1993); F. Bernardini, V. Fiorentini, and D. Vanderbilt, *ibid.* **56**, R10024 (1997); R. Resta, *Rev. Mod. Phys.* **66**, 899 (1994); E. J. Mele and P. Král, *Phys. Rev. Lett.* **88**, 056803 (2002).
 - [2] D. Xiao, M. C. Chang, and Q. Niu, *Rev. Mod. Phys.* **82**, 1959 (2010).
 - [3] N. Marzari, A. A. Mostofi, J. R. Yates, I. Souza, and D. Vanderbilt, *Rev. Mod. Phys.* **84**, 1419 (2012).
 - [4] M. Droth, G. Burkard, and V. M. Pereira, *Phys. Rev. B* **94**, 075404 (2016).
 - [5] J. Li, Y. Wang, Z. Wang, J. Tan, B. Wang, and Y. Liu, *Phys. Rev. B* (to be published), arXiv:1708.00384.
 - [6] H. Rostami, F. Guinea, M. Polini, and R. Roldán, *npj 2D Mater. Appl.* **2**, 15 (2018).
 - [7] D. J. Thouless, M. Kohmoto, M. P. Nightingale, and M. den Nijs, *Phys. Rev. Lett.* **49**, 405 (1982); F. D. M. Haldane, *ibid.* **61**, 2015 (1988); X. G. Wen, *Int. J. Mod. Phys. B* **05**, 1641 (1991).
 - [8] M. Z. Hasan and C. L. Kane, *Rev. Mod. Phys.* **82**, 3045 (2010); X. L. Qi and S. C. Zhang, *ibid.* **83**, 1057 (2011); A. Bansil, H. Lin, and T. Das, *ibid.* **88**, 021004 (2016); C. K. Chiu, J. C. Y. Teo, A. P. Schnyder, and S. Ryu, *ibid.* **88**, 035005 (2016); K. He, Y. Wang, and Q.-K. Xue, *Natl. Sci. Rev.* **1**, 38 (2014); Y. Ando and L. Fu, *Annu. Rev. Condens. Matter Phys.* **6**, 361 (2015).
 - [9] K. A. N. Duerloo, M. T. Ong, and E. J. Reed, *J. Phys. Chem. Lett.* **3**, 2871 (2012).
 - [10] M. N. Blonsky, H. L. Zhuang, A. K. Singh, and R. G. Hennig, *ACS Nano* **9**, 9885 (2015).
 - [11] M. M. Alyörük, Y. Aierken, D. Çakir, F. M. Peeters, and C. Sevik, *J. Phys. Chem. C* **119**, 23231 (2015); L. Dong, J. Lou, and V. B. Shenoy, *ACS Nano* **11**, 8242 (2017); Y. Guo, S. Zhou, Y. Bai, and J. Zhao, *Appl. Phys. Lett.* **110**, 163102 (2017).
 - [12] L. Huang, Y. Li, Z. Wei, and J. Li, *Sci. Rep.* **5**, 16448 (2015); M. Wu, S. Dong, K. Yao, J. Liu, and X. C. Zeng, *Nano Lett.* **16**, 7309 (2016).
 - [13] R. Fei, W. Li, J. Li, and L. Yang, *Appl. Phys. Lett.* **107**, 173104 (2015); L. C. Gomes, A. Carvalho, and A. H. Castro Neto, *Phys. Rev. B* **92**, 214103 (2015).
 - [14] M. T. Ong and E. J. Reed, *ACS Nano* **6**, 1387 (2012); S. I. Kundalwal, S. A. Meguid, and G. J. Weng, *Carbon* **117**, 462 (2017).
 - [15] K. H. Michel, D. Çakir, C. Sevik, and F. M. Peeters, *Phys. Rev. B* **95**, 125415 (2017).
 - [16] W. Wu, L. Wang, Y. Li, F. Zhang, L. Lin, S. Niu, D. Chenet, X. Zhang, Y. Hao, T. F. Heinz, J. Hone, and Z. L. Wang, *Nature (London)* **514**, 470 (2014).
 - [17] H. Zhu, Y. Wang, J. Xiao, M. Liu, S. Xiong, Z. J. Wong, Z. Ye, Y. Ye, X. Yin, and X. Zhang, *Nat. Nanotechnol.* **10**, 151 (2015).
 - [18] S. Manzeli, A. Allain, A. Ghadimi, and A. Kis, *Nano Lett.* **15**, 5330 (2015); A. R. Rezk, B. Carey, A. F. Chrimes, D. W. M. Lau, B. C. Gibson, C. Zheng, M. S. Fuhrer, L. Y. Yeo, and K. Kalantar-zadeh, *ibid.* **16**, 849 (2016); C. J. Brennan, R. Ghosh, K. Koul, S. K. Banerjee, N. Lu, and E. T. Yu, *ibid.* **17**, 5464 (2017); J. Qi, Y. W. Lan, A. Z. Stieg, J. H. Chen, Y. L. Zhong, L. J. Li, C. D. Chen, Y. Zhang, and K. L. Wang, *Nat. Commun.* **6**, 7430 (2015); S. K. Kim, R. Bhatia, T. H. Kim, D. Seol, J. H. Kim, H. Kim, W. Seung, Y. Kim, Y. H. Lee, and S. W. Kim, *Nano Energy* **22**, 483 (2016); W. Wu, L. Wang, R. Yu, Y. Liu, S. H. Wei, J. Hone, and Z. L. Wang, *Adv. Mater.* **28**, 8463 (2016); X. Song, F. Hui, K. Gilmore, B. Wang, G. Jing, Z. Fan,

- E. Grustan-Gutierrez, Y. Shi, L. Lombardi, S. A. Hodge, A. C. Ferrari, and M. Lanza, *Nanoscale* **9**, 6237 (2017).
- [19] S. Chandratre and P. Sharma, *Appl. Phys. Lett.* **100**, 023114 (2012); X. Wang, H. Tian, W. Xie, Y. Shu, W. T. Mi, M. A. Mohammad, Q. Y. Xie, Y. Yang, J. B. Xu, and T. L. Ren, *NPJ Asia Mater.* **7**, e154 (2015); G. d. C. Rodrigues, P. Zelenovskiy, K. Romanyuk, S. Luchkin, Y. Kopelevich, and A. Khoklin, *Nat. Commun.* **6**, 7572 (2015).
- [20] M. Zelisko, Y. Hanlumyuang, S. Yang, Y. Liu, C. Lei, J. Li, P. M. Ajayan, and P. Sharma, *Nat. Commun.* **5**, 4284 (2014).
- [21] Y. Zhou, D. Wu, Y. Zhu, Y. Cho, Q. He, X. Yang, K. Herrera, Z. Chu, Y. Han, M. C. Downer, H. Peng, and K. Lai, *Nano Lett.* **17**, 5508 (2017).
- [22] B. Radisavljevic, A. Radenovic, J. Brivio, V. Giacometti, and A. Kis, *Nat. Nanotechnol.* **6**, 147 (2011).
- [23] K. F. Mak, C. Lee, J. Hone, J. Shan, and T. F. Heinz, *Phys. Rev. Lett.* **105**, 136805 (2010); A. Splendiani, L. Sun, Y. Zhang, T. Li, J. Kim, C. Y. Chim, G. Galli, and F. Wang, *Nano Lett.* **10**, 1271 (2010).
- [24] Q. H. Wang, K. Kalantar-Zadeh, A. Kis, J. N. Coleman, and M. S. Strano, *Nat. Nanotechnol.* **7**, 699 (2012); S. Mao, J. Chang, H. Pu, G. Lu, Q. He, H. Zhang, and J. Chen, *Chem. Soc. Rev.* **46**, 6872 (2017); S. Manzeli, D. Ovchinnikov, D. Pasquier, O. V. Yazyev, and A. Kis, *Nat. Rev. Mater.* **2**, 17033 (2017).
- [25] Z. Zhu, Y. Cheng, and U. Schwingenschlögl, *Phys. Rev. B* **84**, 153402 (2011).
- [26] D. Xiao, G. B. Liu, W. Feng, X. Xu, and W. Yao, *Phys. Rev. Lett.* **108**, 196802 (2012); T. Cao, G. Wang, W. Han, H. Ye, C. Zhu, J. Shi, Q. Niu, P. Tan, E. Wang, B. Liu, and J. Feng, *Nat. Commun.* **3**, 887 (2012); H. Zeng, J. Dai, W. Yao, D. Xiao, and X. Cui, *Nat. Nanotechnol.* **7**, 490 (2012).
- [27] K. F. Mak and J. Shan, *Nat. Photon.* **10**, 216 (2016); J. R. Schaibley, H. Yu, G. Clark, P. Rivera, J. S. Ross, K. L. Seyler, W. Yao, and X. Xu, *Nat. Rev. Mater.* **1**, 16055 (2016).
- [28] S. Bertolazzi, J. Brivio, and A. Kis, *ACS Nano* **5**, 9703 (2011); D. Lloyd, X. Liu, N. Boddeti, L. Cantley, R. Long, M. L. Dunn, and J. Scott Bunch, *Nano Lett.* **17**, 5329 (2017).
- [29] J. Lee, Z. Wang, K. He, J. Shan, and P. X. L. Feng, *ACS Nano* **7**, 6086 (2013).
- [30] J. A. Rogers, T. Someya, and Y. Huang, *Science* **327**, 1603 (2010).
- [31] M. A. Cazalilla, H. Ochoa, and F. Guinea, *Phys. Rev. Lett.* **113**, 077201 (2014).
- [32] H. Rostami, R. Roldán, E. Cappelluti, R. Asgari, and F. Guinea, *Phys. Rev. B* **92**, 195402 (2015).
- [33] A. J. Pearce, E. Mariani, and G. Burkard, *Phys. Rev. B* **94**, 155416 (2016).
- [34] H. Ochoa, R. Zarzuela, and Y. Tserkovnyak, *Phys. Rev. Lett.* **118**, 026801 (2017).
- [35] H. Suzuura and T. Ando, *Phys. Rev. B* **65**, 235412 (2002); J. L. Mañes, *ibid.* **76**, 045430 (2007); F. Guinea, B. Horovitz, and P. Le Doussal, *ibid.* **77**, 205421 (2008); V. M. Pereira and A. H. Castro Neto, *Phys. Rev. Lett.* **103**, 046801 (2009).
- [36] H. Z. Lu, W. Yao, D. Xiao, and S. Q. Shen, *Phys. Rev. Lett.* **110**, 016806 (2013).
- [37] X. Li, J. T. Mullen, Z. Jin, K. M. Borysenko, M. Buongiorno Nardelli, and K. W. Kim, *Phys. Rev. B* **87**, 115418 (2013); T. Gunst, T. Markussen, K. Stokbro, and M. Brandbyge, *ibid.* **93**, 035414 (2016).
- [38] N. F. Hinsche, A. S. Ngankeu, K. Guilloy, S. K. Mahatha, A. Grubisic Cabo, M. Bianchi, M. Dendzik, C. E. Sanders, J. A. Miwa, H. Bana, E. Travaglia, P. Lacovig, L. Bignardi, R. Larciprete, A. Baraldi, S. Lizzit, K. S. Thygesen, and P. Hofmann, *Phys. Rev. B* **96**, 121402(R) (2017).
- [39] S. Tongay, J. Zhou, C. Ataca, K. Lo, T. S. Matthews, J. Li, J. C. Grossman, and J. Wu, *Nano Lett.* **12**, 5576 (2012); P. Dey, J. Paul, Z. Wang, C. E. Stevens, C. Liu, A. H. Romero, J. Shan, D. J. Hilton, and D. Karaiskaj, *Phys. Rev. Lett.* **116**, 127402 (2016).
- [40] Y. Song and H. Dery, *Phys. Rev. Lett.* **111**, 026601 (2013).
- [41] J. Lee, Z. Wang, H. Xie, K. F. Mak, and J. Shan, *Nat. Mater.* **16**, 887 (2017).
- [42] H. J. Conley, B. Wang, J. I. Ziegler, R. F. Haglund, S. T. Pantelides, and K. I. Bolotin, *Nano Lett.* **13**, 3626 (2013).
- [43] S. Horzum, H. Sahin, S. Cahangirov, P. Cudazzo, A. Rubio, T. Serin, and F. M. Peeters, *Phys. Rev. B* **87**, 125415 (2013).
- [44] W. S. Yun, S. W. Han, S. C. Hong, I. G. Kim, and J. D. Lee, *Phys. Rev. B* **85**, 033305 (2012); H. Peelaers and C. G. Van de Walle, *ibid.* **86**, 241401(R) (2012); H. Shi, H. Pan, Y. W. Zhang, and B. I. Yakobson, *ibid.* **87**, 155304 (2013); M. Ghorbani-Asl, S. Borini, A. Kuc, and T. Heine, *ibid.* **87**, 235434 (2013); Y. Ge, W. Wan, W. Feng, D. Xiao, and Y. Yao, *ibid.* **90**, 035414 (2014); Q. Yue, J. Kang, Z. Shao, X. Zhang, S. Chang, G. Wang, S. Qin, and J. Li, *Phys. Lett. A* **376**, 1166 (2012); P. Johari and V. B. Shenoy, *ACS Nano* **6**, 5449 (2012); P. Lu, X. Wu, W. Guo, and X. C. Zeng, *Phys. Chem. Chem. Phys.* **14**, 13035 (2012); K. He, C. Poole, K. F. Mak, and J. Shan, *Nano Lett.* **13**, 2931 (2013).
- [45] A. Castellanos-Gómez, R. Roldán, E. Cappelluti, M. Buscema, F. Guinea, H. S. J. van der Zant, and G. A. Steele, *Nano Lett.* **13**, 5361 (2013); G. H. Ahn, M. Amani, H. Rasool, D.-H. Lien, J. P. Mastandrea, J. W. Ager III, M. Dubey, D. C. Chrzan, A. M. Minor, and A. Javey, *Nat. Commun.* **8**, 608 (2017).
- [46] N. A. Lanzillo, A. J. Simbeck, and S. K. Nayak, *J. Phys.: Condens. Matter* **27**, 175501 (2015); L. Yu, A. Ruzsinszky, and J. P. Perdew, *Nano Lett.* **16**, 2444 (2016).
- [47] G. B. Liu, W. Y. Shan, Y. Yao, W. Yao, and D. Xiao, *Phys. Rev. B* **88**, 085433 (2013).
- [48] E. Cappelluti, R. Roldán, J. A. Silva-Guillén, P. Ordejón, and F. Guinea, *Phys. Rev. B* **88**, 075409 (2013); S. Fang, R. Kuate Defo, S. N. Shirodkar, S. Lieu, G. A. Tritsaris, and E. Kaxiras, *ibid.* **92**, 205108 (2015); F. Zahid, L. Liu, Y. Zhu, J. Wang, and H. Guo, *AIP Adv.* **3**, 052111 (2013).
- [49] A. H. Castro Neto, F. Guinea, N. M. R. Peres, K. S. Novoselov, and A. K. Geim, *Rev. Mod. Phys.* **81**, 109 (2009).
- [50] L. Li, E. V. Castro, and P. D. Sacramento, *Phys. Rev. B* **94**, 195419 (2016).
- [51] F. Giustino, *Rev. Mod. Phys.* **89**, 015003 (2017).
- [52] L. Pietronero, S. Strässler, H. R. Zeller, and M. J. Rice, *Phys. Rev. B* **22**, 904 (1980); R. A. Jishi, M. S. Dresselhaus, and G. Dresselhaus, *ibid.* **48**, 11385 (1993).
- [53] B. Amorim, A. Cortijo, F. de Juan, A. G. Grushin, F. Guinea, A. Gutiérrez-Rubio, H. Ochoa, V. Parente, R. Roldán, P. San-José, J. Schiefele, M. Sturla, and M. A. H. Vozmediano, *Phys. Rep.* **617**, 1 (2016).
- [54] G. G. Naumis, S. Barraza-Lopez, M. Oliva-Leyva, and H. Terrones, *Rep. Prog. Phys.* **80**, 096501 (2017).
- [55] P. O. Löwdin, *J. Chem. Phys.* **19**, 1396 (1951).
- [56] A. Kormányos, G. Burkard, M. Gmitra, J. Fabian, V. Zólyomi, N. D. Drummond, and V. Fal’ko, *2D Mater.* **2**, 022001 (2015).

- [57] A. Kormányos, V. Zolyomi, N. D. Drummond, P. Rakyta, G. Burkard, and V. I. Fal'ko, *Phys. Rev. B* **88**, 045416 (2013).
- [58] M. A. H. Vozmediano, M. I. Katsnelson, and F. Guinea, *Phys. Rep.* **496**, 109 (2010).
- [59] M. R. Masir, D. Moldovan, and F. Peeters, *Solid State Commun.* **175-176**, 76 (2013).
- [60] S. T. Gill, J. H. Hinnefeld, S. Zhu, W. J. Swanson, T. Li, and N. Mason, *ACS Nano* **9**, 5799 (2015).
- [61] N. C. Yeh, C. C. Hsu, M. L. Teague, J. Q. Wang, D. A. Boyd, and C. C. Chen, *Acta Mech. Sin.* **32**, 497 (2016).
- [62] C. Si, Z. Sun, and F. Liu, *Nanoscale* **8**, 3207 (2016).
- [63] D. Akinwande, C. J. Brennan, J. S. Bunch, P. Egberts, J. R. Felts, H. Gao, R. Huang, J.-S. Kim, T. Li, Y. Li, K. M. Liechti, N. Lu, H. S. Park, E. J. Reed, P. Wang, B. I. Yakobson, T. Zhang, Y. W. Zhang, Y. Zhou, and Y. Zhu, *Extreme Mech. Lett.* **13**, 42 (2017).
- [64] F. Zhai, X. Zhao, K. Chang, and H. Q. Xu, *Phys. Rev. B* **82**, 115442 (2010).
- [65] T. Low and F. Guinea, *Nano Lett.* **10**, 3551 (2010).
- [66] Y. Jiang, T. Low, K. Chang, M. I. Katsnelson, and F. Guinea, *Phys. Rev. Lett.* **110**, 046601 (2013).
- [67] Z. Qi, A. L. Kitt, H. S. Park, V. M. Pereira, D. K. Campbell, and A. H. Castro Neto, *Phys. Rev. B* **90**, 125419 (2014).
- [68] B. Wang, Y. Wang, and Y. Liu, *Funct. Mater. Lett.* **08**, 1530001 (2015).
- [69] G. J. Verbiest, S. Brinker, and C. Stampfer, *Phys. Rev. B* **92**, 075417 (2015).
- [70] M. Settnes, S. R. Power, and A.-P. Jauho, *Phys. Rev. B* **93**, 035456 (2016).
- [71] Q. Zhang, Y. Cheng, L.-Y. Gan, and U. Schwingenschlögl, *Phys. Rev. B* **88**, 245447 (2013).
- [72] C. R. Zhu, G. Wang, B. L. Liu, X. Marie, X. F. Qiao, X. Zhang, X. X. Wu, H. Fan, P. H. Tan, T. Amand, and B. Urbaszek, *Phys. Rev. B* **88**, 121301 (2013).
- [73] D. Lu, I. M. Vishik, M. Yi, Y. Chen, R. G. Moore, and Z.-X. Shen, *Annu. Rev. Condens. Matter Phys.* **3**, 129 (2012).
- [74] T. Hertel and G. Moos, *Phys. Rev. Lett.* **84**, 5002 (2000).
- [75] N. Levy, S. A. Burke, K. L. Meaker, M. Panlasigui, A. Zettl, F. Guinea, A. H. Castro Neto, and M. F. Crommie, *Science* **329**, 544 (2010); J. Lu, A. H. Castro Neto, and K. P. Loh, *Nat. Commun.* **3**, 823 (2012).
- [76] S. Zhu, J. A. Stroscio, and T. Li, *Phys. Rev. Lett.* **115**, 245501 (2015).
- [77] F. Guinea, M. I. Katsnelson, and A. K. Geim, *Nat. Phys.* **6**, 30 (2010).
- [78] N. N. Klimov, S. Jung, S. Zhu, T. Li, C. A. Wright, S. D. Solares, D. B. Newell, N. B. Zhitenev, and J. A. Stroscio, *Science* **336**, 1557 (2012); D. Guo, T. Kondo, T. Machida, K. Iwatake, S. Okada, and J. Nakamura, *Nat. Commun.* **3**, 1068 (2012).
- [79] S. Fang, S. Carr, J. Shen, M. A. Cazalilla, and E. Kaxiras, *Phys. Rev. B* **98**, 075106 (2018).